Common-Mode Current Elimination PWM Strategy Along With Current Ripple Reduction for Open-Winding Five-Phase Induction Motor Drive

Ramsha Karampuri, Sachin Jain, *Senior Member, IEEE*, and V. T. Somasekhar, *Member, IEEE*

***Abstract*—The three-level dual-inverter connected to five-phase open-end winding induction motor (FPOEWIM) drive with a single dc source results in the flow of common mode current (CMC). The CMC flows through the common dc bus connected to dual-inverter and the motor phase windings. The CMC can be eliminated by using the switching states that can generate zero common mode voltage (CMV). In case of FPOEWIM, these switching states may result in higher current ripple. This paper proposes a decoupled pulsewidth modulation (PWM) technique to reduce the motor phase current ripple by using nearest possible space vector locations (SVLs) with zero as well as non-zero CMV. The use of non-zero CMV states results in CMC. So, the CMC is averaged to zero using sample-averaged common-mode current elimination (SACE) PWM technique in conjunction with decoupled PWM, which is named as DSACE PWM technique. Furthermore, the application of the proposed PWM is also supported using simulation for the closed-loop control scheme, such as DTC. Also, the proposed decoupled and DSACE PWM techniques are verified experimentally and the results are compared with the conventional 144° decoupled PWM technique.**

***Index Terms*—Common mode current (CMC), common mode voltage (CMV), five-phase induction motor, open-end winding (OEW) topology, pulsewidth modulation (PWM) technique.**

I. Introduction

EXTENSIVE research work is being carried out throughout the world to improve the performance of an electric drive system for medium- and high-power electric applications. Such applications include electric vehicles, hybrid electric vehicles, rolling mills, electric ship propulsion, wind energy systems, etc. Most of the researchers have suggested the use of multi-phase machines for these medium- and high-power applications [1]–[4]. Multi-phase drives have the advantages of higher fault-tolerance [5], reduced torque ripple, reduced per phase current without increasing the per phase voltage, etc. They also reduce the VA rating of power electronic switches used in the converters because of the reduced per phase current [6], [7]. Furthermore, the overall performance of the drive system may also be improved with the use of multi-level inverter [8], [9].

A few authors have investigated the multi-phase, multi-level drives, especially with open-end winding (OEW) configuration [10]–[13]. The five-phase three-level dual-inverter with OEW configuration has attracted many researchers, owing to the advantages, such as the absence of neutral point fluctuations, redundancy in the switching states, etc. [14]. The OEW configuration also allows the use of either a single source (i.e., a common dc bus) or two isolated sources with separate dc links. This paper uses a single source connected to dual-inverter through a common dc bus, which could avoid the use of bulky isolation transformers [15]. The use of common dc bus could result in the flow of common mode current (CMC), which is undesired as in the case of the three-phase drive system. Since the CMC do not contribute in the electro-mechanical energy conversion but heats up the machine windings [16]. Also, the common mode voltage (CMV) coupling through motor parasitic capacitance creates shaft voltages, which can lead to premature bearing failure.

In the case of three-phase OEW induction motor (OEWIM) drive system with single dc source, many investigations were reported to eliminate or suppress the CMC [16]–[23]. The basic approach to eliminate the CMC from the common dc bus and the motor windings is to operate both the inverters with 120° (i.e., 360°/3) phase displacement [16], [17]. This pulsewidth modulation (PWM) technique [16], [17] uses only those space vector combinations that could generate zero CMV. Hence, this results in the underutilization of the available space vector locations (SVLs) [18]. To improve the utilization of the SVLs, another PWM technique was proposed in [18]–[21], wherein the CMC is averaged to zero within a sampling time interval. This technique can be named as sample-averaged common-mode current elimination (SACE) PWM technique. However, the SACE PWM technique for three-phase drive results in higher current ripple, which was reduced using the decoupled SACE (DSACE) PWM technique, as presented in [22] and [23].

Similarly, in the case of five-phase OEWIM (FPOEWIM) drive with the common dc bus, both of the five-phase two-level inverters could be operated with the phase displacement of either 72° (i.e., 360°/5) or 144° (i.e., 2 × 360°/5) to eliminate CMC [11], [13]. The phase displacement of 72° between both the inverters could result in poor dc bus utilization, whereas the

Manuscript received April 16, 2018; revised August 12, 2018; accepted September 18, 2018. Date of publication October 3, 2018; date of current version May 2, 2019. Recommended for publication by Associate Editor Prof. K.-B. Lee. *(Corresponding author: Sachin Jain.)*

R. Karampuri is with the Department of Electrical and Electronics Engineering, SR Engineering College, Warangal 506371, India (e-mail: ramsha.karampuri@gmail.com).

S. Jain and V. T. Somasekhar are with the Department of Electrical Engineering, National Institute of Technology, Warangal 506004, India (e-mail: jsachin@nitw.ac.in; sekhar@nitw.ac.in).

Color versions of one or more of the figures in this paper are available online at http://ieeexplore.ieee.org.

Digital Object Identifier 10.1109/TPEL.2018.2873692

144° decoupled PWM technique gives better dc bus utilization than the former. However, this technique uses the space vector combinations for which the CMV is zero. The number of space vector combinations in case of the five-phase dual inverter is 1024. Out of which, only 22 space vector combinations could be used in case of 144° decoupled PWM technique. Hence, resulting in the under utilization of the available space vector combinations. In addition, the farther SVLs are to be used to realize the reference voltage vector, which may result in the higher ripple content in the motor phase current [24]. A similar SACE PWM technique for FPOEWIM drive was proposed in [25], which is the extension from the three-phase OEWIM drive. This technique could also lead to the higher current ripple in the motor phase current.

This paper proposes the decoupled PWM technique, where the reference voltage vectors of inverter-I and inverter-II are phase displaced by 180°. The phase displacement of 180° between both of the inverters helps in reducing the required dc bus voltage, since both of the reference voltage vectors are added to generate the required motor phase voltage [22]. In addition, the proposed PWM technique uses the nearest SVLs for which the CMV is zero as well as non-zero. This results in the minimization of ripple in the motor phase current. But, the decoupled PWM technique induces the CMC into the motor windings because of the use of non-zero CMV SVLs.

To eliminate the CMC, the DSACE PWM technique [22] is extended to FPOEWIM drive and is presented in this paper. The DSACE PWM technique for five-phase drive system is quite complex when compared to that of a three-phase system, because of the large number of space vector combinations and locations. The above-discussed decoupled PWM technique is combined with the SACE PWM technique, wherein the variation of the effective time period (the time period for which only the active vectors are realized) is used [18]. The variation of the effective time period within a sampling time interval could nullify the CMV in the average sense and thereby eliminate the CMC.

In the following sections, a brief explanation of the system modeling is presented followed by the explanation and analysis of both the proposed decoupled and DSACE PWM techniques. Thereafter, the simulation results along with the experimental verification are furnished. Later, the conclusions from both the PWM techniques are presented in the last section.

II. System Modeling

The circuit schematic of the considered topology with a single dc source connected to a three-level dual-inverter fed FPOEWIM drive is shown in Fig. 1. The dual-inverter consists of 20 switches in 10 legs (namely $a, b, c, d, e, a', b', c', d'$, and e'), which are connected to the either ends of FPOEWIM forming the phases $aa', bb', cc', dd',$ and ee'. The mathematical model of symmetrical distributed wound FPOEWIM is considered in this paper. The windings are equally displaced by an angle $\theta = 2\pi/5$ with the neutral point opened. The motor model is constructed by considering all the standard assumptions of the general theory of electrical machines. The machine model is represented

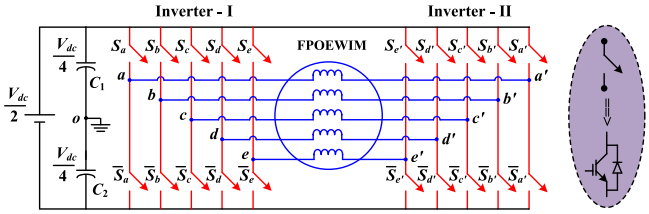

Fig. 1. Three-level dual-inverter connected five-phase open-end winding induction motor drive with single dc source.

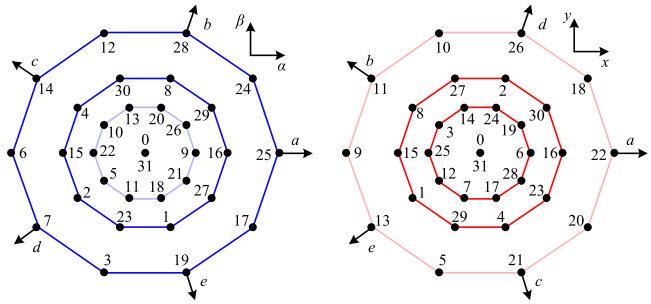

Fig. 2. Space vector locations and switching states for inverter-I in $\alpha - \beta$ and $x - y$ subspaces.

by a set of stator and rotor phase voltage equilibrium equations referred to a fixed reference frame linked to the stator as

$$\vec{v}_{kj} = r_j \vec{i}_{kj} + p\vec{\lambda}_{kj} \tag{1}$$

where $j = s$ for stator and r for rotor; $k = \{aa', bb', cc', dd', ee'\}$; $\vec{x}_{kj} = x_{aa'j}\ x_{bb'j}\ x_{cc'j}\ x_{dd'j}\ x_{ee'j}]^T$; $x = \{v$ (voltage), i (current), λ (flux linkage)$\}$; $\vec{r}_j = \text{diag}[r_j\ r_j\ r_j\ r_j\ r_j]$; and p is the time derivative.

The algebraic flux-linkage equation (2) is obtained from the current flowing through the motor phases, the self and mutual inductances of machine winding represented as L

$$\vec{\lambda}_{kj} = \vec{L}\vec{i}_{kj}. \tag{2}$$

The machine model given in (1) and (2) is decoupled into two orthogonal subspaces ($\alpha - \beta$ and $x - y$ subspaces) using the Clarke transformation detailed as follows:

$$\vec{C} = \sqrt{\frac{2}{5}} \begin{bmatrix} 1 & \cos\theta & \cos 2\theta & \cos 3\theta & \cos 4\theta \\ 0 & \sin\theta & \sin 2\theta & \sin 3\theta & \sin 4\theta \\ 1 & \cos 2\theta & \cos 4\theta & \cos 6\theta & \cos 8\theta \\ 0 & \sin 2\theta & \sin 4\theta & \sin 6\theta & \sin 8\theta \\ 1/\sqrt{2} & 1/\sqrt{2} & 1/\sqrt{2} & 1/\sqrt{2} & 1/\sqrt{2} \end{bmatrix} \begin{matrix} \alpha \\ \beta \\ x \\ y \\ 0. \end{matrix} \tag{3}$$

The $\alpha - \beta$ subspace represents the fundamental components responsible for the generation of torque, whereas the $x - y$ subspace includes the third harmonic components that do not contribute to the torque production in a distributed wound FPOEWIM [26]. Fig. 2 shows the SVLs and switching states in $\alpha - \beta$ and $x - y$ subspaces of inverter-I (similar locations and states exists for inverter-II). There exist three groups of vectors large, medium, and small with the magnitudes $V_{\text{dc}}(\sqrt{5}+1)/10$,

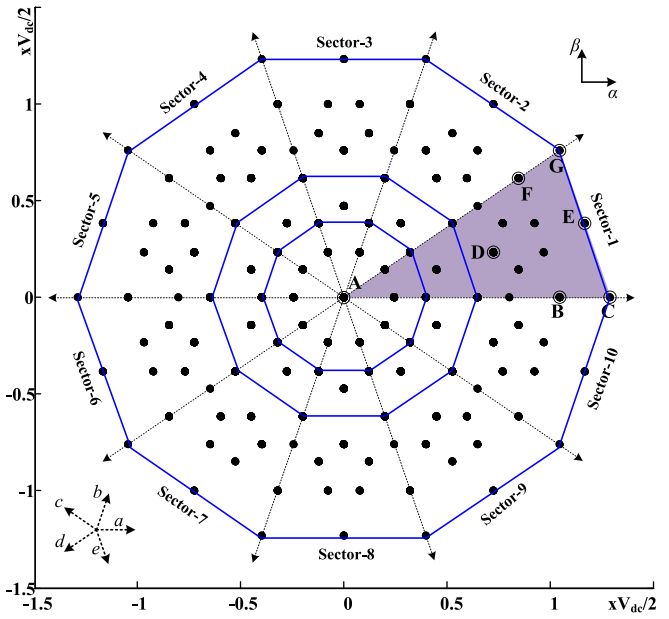

Fig. 3. Space vector locations in $\alpha - \beta$ subspace for the dual-inverter using the medium and large vectors of $\alpha - \beta$ subspace.

$V_{\rm dc}/5$, and $V_{\rm dc}(\sqrt{5}-1)/10$, respectively (for a dc bus voltage of $V_{\rm dc}/\,2$).

The switching states of inverter-I and inverter-II are represented by the vectors $[S_a\ S_b\ S_c\ S_d\ S_e]^T$ and $[S_{a'}\ S_{b'}\ S_{c'}\ S_{d'}\ S_{e'}]^T$, respectively, where $S_l \in \{0, 1\}\,(l = \{a, b, c, d, e, a', b', c', d', e'\})$. $S_l = 0$ indicates that leg l is connected to the negative rail of the dc bus, whereas $S_l = 1$ indicates that leg l is connected to the positive rail of the dc bus. The stator phase voltage v_{ks} is obtained from the switching states and the applied dc bus voltage $V_{\rm dc}/2$ as follows:

$$\begin{bmatrix} v_{aa's} \\ v_{bb's} \\ v_{cc's} \\ v_{dd's} \\ v_{ee's} \end{bmatrix} = \frac{V_{\rm dc}}{10} \begin{bmatrix} 4 & -1 & -1 & -1 & -1 \\ -1 & 4 & -1 & -1 & -1 \\ -1 & -1 & 4 & -1 & -1 \\ -1 & -1 & -1 & 4 & -1 \\ -1 & -1 & -1 & -1 & 4 \end{bmatrix} \begin{bmatrix} (S_a - S_{a'}) \\ (S_b - S_{b'}) \\ (S_c - S_{c'}) \\ (S_d - S_{d'}) \\ (S_e - S_{e'}) \end{bmatrix}. \tag{4}$$

III. Decoupled PWM Technique

In case of a five-phase two-level inverter, the $\alpha - \beta$ and $x - y$ subspaces consist of 31 SVLs and 2^5 $(= 32)$ switching states, as shown in Fig. 2. For a five-phase three-level dual-inverter, there exist 211 SVLs with 2^5x2^5 $(= 1024)$ switching states. To simplify implementation only the medium and large vectors are considered in the proposed decoupled PWM technique. This helps in reducing the third harmonic component that exists in $x - y$ subspace, since the small vectors in $\alpha - \beta$ subspace are mapped as large vectors in $x - y$ subspace and vice versa, whereas the medium vectors remain the same. Furthermore, choosing only the large and medium vectors also helps in minimizing the number of switching states and the SVLs. Fig. 3 shows the space vector diagram in $\alpha - \beta$ subspace for a three-level dual-inverter

TABLE I
Switching States at Selected Space Vector Locations for the Proposed PWM Technique

Space vector location	Possible switching states	Selected Switching states
A	0-0', 1-1', 2-2', 3-3', 4-4', 6-6', 7-7', 8-8', 12-12', 14-14', 15-15', 16-16', 17-17', 19-19', 23-23', 24-24', 25-25', 27-27', 28-28', 29-29', 30-30', 31-31'	0-0', 31-31'
B	16-6', 25-15', 24-14', 17-7'	16-6', 25-15'
C	25-6'	25-6'
D	16-2', 29-15', 28-14', 17-3'	16-2', 29-15'
E	24-6', 25-7'	24-6', 25-7'
F	24-2', 25-3', 29-7', 28-6'	24-2', 29-7'
G	24-7'	24-7'

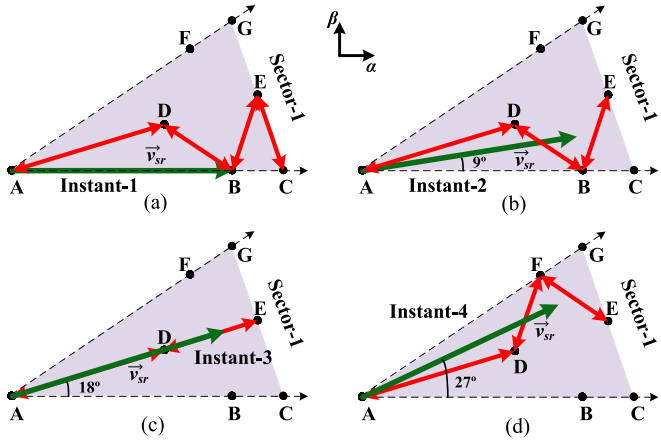

Fig. 4. Switching sequence for realizing the reference voltage vector of the dual-inverter in case of the proposed 180° decoupled PWM. (a) For instant-1. (b) For instant-2. (c) For instant-3. (d) Instant-4 of sector-1.

with large and medium vectors. This results in 131 SVLs and 484 switching states in 10 sectors with a span of $\pi/5$ radians between each sector. The same number of SVLs and switching states can be obtained in $x - y$ subspace, but the large vectors are mapped as small, and the medium remains unchanged.

Consider the sector-1 with the shaded region, as shown in Fig. 3. The proposed decoupled PWM is implemented using the SVLs A, B, C, D, E, F, and G of the shaded sector, as encircled in Fig. 3. The use of switching states at SVLs A, D, and E contribute zero CMV, whereas the switching states at SVLs B, C, F, and G will contribute non-zero CMV. The possible switching states at all these SVLs are furnished in Table I. There is a high redundancy in switching states at location A, which can be realized using 22 switching states. Also, there is a redundancy in the switching states at other locations except for C and G. The switching states used in the proposed decoupled PWM technique are furnished in the last column of Table I.

The switching sequence in the selected sector (i.e., sector-1) is not unique but changes from instant to instant, as shown in Fig. 4. For analysis of the switching sequence, 40 instants per cycle are

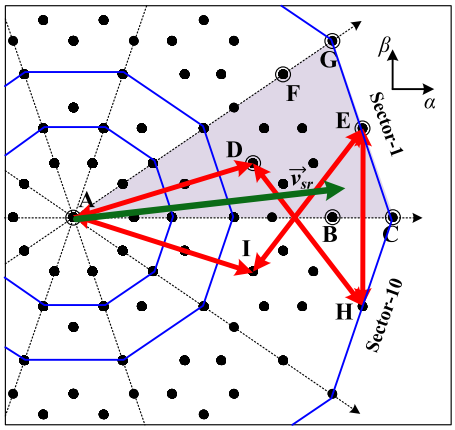

Fig. 5. Switching sequence for realizing the reference voltage vector of the dual-inverter in case of 144° decoupled PWM.

considered (i.e., 4 instants per sector). However, the number of instants per sector could be varied. Considering the first instant (instant-1) where the reference voltage vector, $\vec{v}_{sr}$ is in phase with the reference α-axis, the switching sequence used is A-D-B-E-C-C-E-B-D-A, as shown in Fig. 4(a). Similarly, for instant-2 located at 9° the switching sequence is A-D-B-E-E-B-D-A, for instant-3 located at 18° the switching sequence is A-D-E-E-D-A, and for the instant-4 located at 27°, the switching sequence is A-D-F-E-E-F-D-A. All the above switching sequences are shown in Fig. 4(a) and (d). The SVLs and the switching sequence are selected such that the third harmonic components in the $x-y$ subspace get nullified [24]. For all the remaining sectors, the above-discussed four switching sequences can be repeated with similar SVLs in the respective sectors. From Fig. 4, it can be observed that the farther SVLs are generally avoided to realize the reference voltage vector, this could help in the reduction of current ripple. This statement can be supported by showing the switching trajectory in case of 144° decoupled PWM technique in Fig. 5. Here, in Fig. 5, the SVLs used to realize the reference voltage vector are corresponding to the zero CMV (i.e., SVLs D, E, H, and I) and are farther when compared to that of the proposed 180° decoupled PWM technique.

The decoupled PWM technique discussed above is quite complex, since the switching sequence and the corresponding pattern changes from instant to instant. But, the implementation is simplified by using the unified voltage modulation algorithm proposed in [27] for the three-phase two-level inverter. The unified voltage modulation algorithm is a carrier-based SVPWM technique. This technique is extended to the five-phase two-level inverter and presented in [28]. The unified voltage modulation algorithm for the three-level dual-inverter connected FPOEWIM is briefly discussed ahead.

The reference voltage vector for the dual-inverter is generated using the following equation:

$$|v_{sr}| = m_a V_{\rm dc} \tag{5}$$

where m_a is the modulation index. The proposed PWM technique can be implemented by synthesizing the reference voltage vector into v_{sr1} for inverter-I and v_{sr2} for inverter-II with 180° (decoupled) phase displacement. So

$$|v_{sr}|\angle\delta = \{|v_{sr1}|\angle\delta\} - \{|v_{sr2}|\angle(\pi+\delta)\} \tag{6}$$

where δ is the angle between the $\alpha-$ axis and the reference voltage vector, which varies in steps by 9° (since 40 instants per fundamental cycle are considered).

As the reference voltage vectors for inverter-I and II are phase displaced by 180°, the dc bus voltage required is 50% of $V_{\rm dc}$ required in case of the conventional five-phase two-level inverter. So, the synthesized voltage vectors can be written as

$$\begin{aligned}\vec{v}_{sr1} &= 0.5|v_{sr}|\angle\delta \\ \vec{v}_{sr2} &= 0.5|v_{sr}|\angle(\pi+\delta).\end{aligned} \tag{7}$$

Now, the procedure given in [22] is followed to operate the inverter-I, wherein the concept of imaginary switching time is used. The switching pulses are generated using the imaginary times calculated from the phase voltage references and by providing an offset time, $T_{\rm offset}$ to get the real gating times ($T_{ga}, T_{gb}, T_{gc}, T_{gd}$, and T_{ge}). The value of $T_{\rm offset}$ used in case of the proposed decoupled PWM technique is

$$T_{\rm offset} = \frac{T_0}{2} - T_{\rm min} \tag{8}$$

where T_0 is the time for which a null vector is realized and $T_{\rm min}$ is the minimum imaginary time at a given instant.

The generation of gating times for inverter-II is very simple, where the above-mentioned procedure is not at all required. The gating times for inverter-II can be directly calculated as follows:

$$\begin{aligned}&T_{ga'} = T_s - T_{ga}; T_{gb'} = T_s - T_{gb}; T_{gc'} = T_s - T_{gc} \\ &T_{gd'} = T_s - T_{gd}; T_{ge'} = T_s - T_{ge}\end{aligned} \tag{9}$$

where $T_s\ (=1/f_s)$ is the switching time. The above-calculated gating times for inverter-I and inverter-II are then compared with the carrier wave of the switching frequency f_s and the PWM pulses are generated. The fundamental frequency f of the inverter output or motor phase voltage is calculated as follows:

$$f = \frac{m_a \times f_{\rm rated}}{m_{a,\rm linear}} \tag{10}$$

where $f_{\rm rated}$ is the rated frequency of the motor, i.e., 50 Hz; and $m_{a,\rm linear}$ is the value of the modulation index at the boundary of linear modulation, i.e., 1.05.

The value of $m_{a,\rm linear}$ can be calculated using the switching pattern employed in the proposed decoupled PWM technique. For inverter-I, the sequence of the active vectors in sector-1 is 29-25-24-16, i.e., medium-large-large-medium vectors. The magnitude of the medium vector is 0.4, whereas the magnitude of the large vector is 0.647. The maximum achievable voltage $V_{\rm max}$ using the sequence 29-25-24-16 is given as follows [29]:

$$V_{\rm max} = \frac{0.4^2 + 0.647^2}{0.4 + 0.647}(V_{\rm dc}/2) = 0.5526(V_{\rm dc}/2). \tag{11}$$

Now, the value of $m_{a,\rm linear}$ can be calculated as follows:

$$m_{a,\rm linear} = \frac{V_{\rm max}}{(V_{\rm dc}/2)}\cos(\pi/10) = 0.525. \tag{12}$$

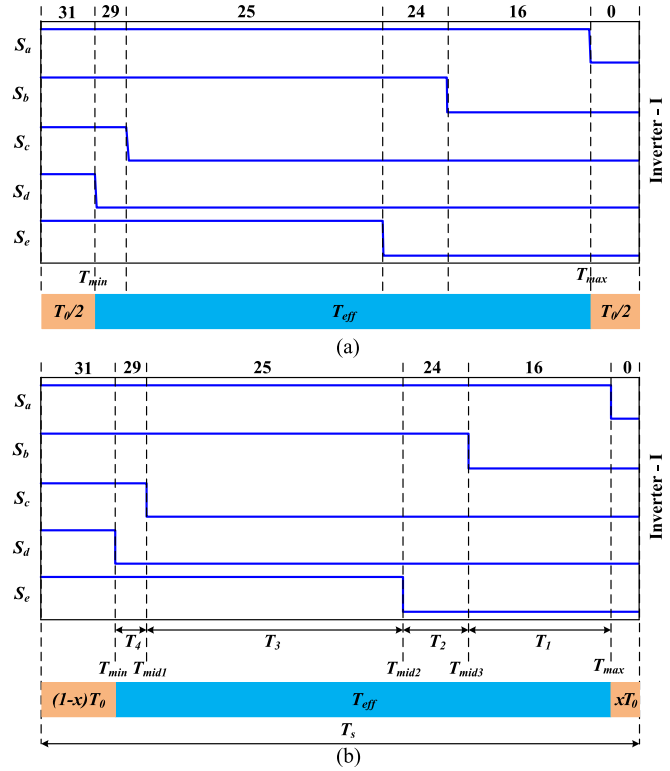

Fig. 6. Gate pulses generated for the inverter-I of five-phase dual-inverter. (a) Using the 180° decoupled PWM technique. (b) Using the DSACE PWM technique.

The value of $m_{a,\text{linear}}$ for the dual-inverter could be directly doubled (i.e., 1.05), since both the inverters are operated with 180° phase displacement.

IV. DSACE PWM Technique

The decoupled PWM technique uses the offset time given in (8), which results in centre spaced effective time, T_{eff} (effective time is the time difference between the maximum $T_{\max}$ and the minimum $T_{\min}$ imaginary times), as shown in Fig. 6(a). In other words, the null vectors are realized in equal time intervals, i.e., $T_0/2$. The value of T_{offset} can be varied or the effective time region can be moved within the span of T_s, as presented in [22] for a three-phase OEWIM drive. This could yield better performance and helps in nullifying the CMC flowing through the common dc bus connected to the dual inverter.

The concept of making the CMC zero in the average sense is extended to FPOEWIM drive and is presented in this section as the DSACE PWM technique. Consider the switching sequence for instant-1, as shown in Fig. 4(a), and the switching pattern is shown in Fig. 6(a). For inverter-I, the switching states used are 31-29-25-24-16-0, which are realized with the switching times $T_0/2 - T_4 - T_3 - T_2 - T_1 - T_0/2$, respectively. The switching sequence and the pattern mentioned in the decoupled PWM technique are unaltered, since the switching times T_1, T_2, T_3, and T_4 are unchanged. The effective time region can be moved by changing only the zero time, T_0, i.e., $(1-x)T_0$ for realizing the switching state "31" and xT_0 (the resultant being T_0) for realizing the switching state "0," as shown in Fig. 6(b). The new offset time results in

TABLE II
CMVs Corresponding to the Switching States Shown in Fig. 6

Switching State	31	29	25	24	16	0
CMV	$-V_{dc}/4$	$-3V_{dc}/20$	$-V_{dc}/20$	$V_{dc}/20$	$3V_{dc}/20$	$V_{dc}/4$

$$T_{\text{offset\_new}} = T_0 - xT_0 - T_{\min}. \tag{13}$$

The value of xT_0 can be derived by forcing the instant-averaged CMV to zero. The CMVs corresponding to the switching states shown in Fig. 6 is furnished in Table II (for dc bus voltage as $V_{\text{dc}}/2$).

The instant-averaged CMV that is averaged to T_s and equated to zero is given by

$$\frac{V_{\text{dc}}}{T_s}\left[\frac{-(1-x)T_0}{4} - \frac{3T_4}{20} - \frac{T_3}{20} + \frac{T_2}{20} + \frac{3T_1}{20} + \frac{xT_0}{4}\right] = 0$$

$$\Rightarrow\ xT_0 = \frac{T_0}{2} + \frac{3}{10}[T_4 - T_1] + \frac{1}{10}[T_3 - T_2]. \tag{14}$$

Now, from Fig. 6(b)

$$T_1 = T_{\max} - T_{\text{mid3}};\ T_2 = T_{\text{mid3}} - T_{\text{mid2}}$$
$$T_3 = T_{\text{mid2}} - T_{\text{mid1}};\ T_4 = T_{\text{mid1}} - T_{\min}. \tag{15}$$

So

$$T_4 - T_1 = 2T_{\text{mid1}} + T_{\text{mid2}} + 2T_{\text{mid3}}$$
$$T_3 - T_2 = -T_{\text{mid1}} + 2T_{\text{mid2}} - T_{\text{mid3}}$$
$$(\because\ T_{\max} + T_{\text{mid1}} + T_{\text{mid2}} + T_{\text{mid3}} + T_{\min} = 0). \tag{16}$$

Substituting (16) in (14) gives

$$xT_0 = \frac{T_0}{2} + \frac{1}{2}(T_{\text{mid1}} + T_{\text{mid2}} + T_{\text{mid3}})$$
$$= \frac{T_0}{2} - \frac{T_{\max} + T_{\min}}{2}. \tag{17}$$

Now, substituting (17) in (13) results in

$$T_{\text{offset\_new}} = \frac{T_0}{2} + \frac{T_{\max} - T_{\min}}{2}$$
$$= (T_0 + T_{\text{eff}})/2\ \ (\because\ T_{\text{eff}} = T_{\max} - T_{\min}) \tag{18}$$

$$T_{\text{offset\_new}} = \frac{T_s}{2}\ \ (\because\ T_s = T_0 + T_{\text{eff}}). \tag{19}$$

The calculated new offset time $T_{\text{offset\_new}}$ is now used to move the region of the effective time period that could help in nullifying the CMC flowing through the common dc bus and the motor phase windings.

The gate pulses for inverter-I and inverter-II (see Fig. 1) are generated using both the proposed decoupled and DSACE PWM techniques, as shown in Fig. 7. Furthermore, the proposed PWM technique in conjunction with the closed-loop direct torque control (DTC) technique [30] is implemented using the schematic block diagram shown in Fig. 8. The shaft speed of the FPOEWIM is sensed and compared with the reference speed

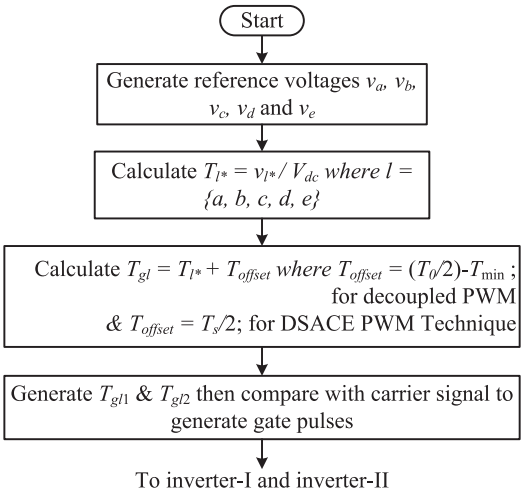

Fig. 7. Flowchart of the proposed decoupled and DSACE PWM techniques to operate inverter-I and inverter-II.

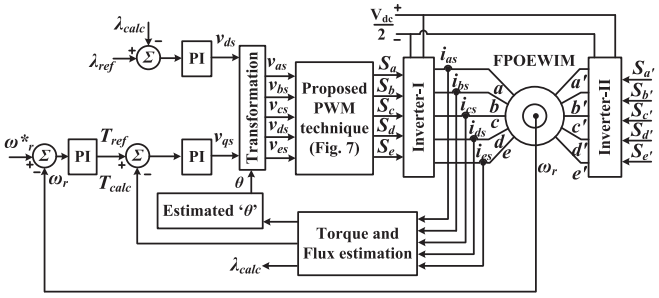

Fig. 8. Schematic block diagram of DTC technique in conjunction with the proposed DSACE PWM.

and the obtained error signal is processed with the PI controller (proportional gain $K_p = 2$ and integral time $T_i = 0.13$) to obtain T_{ref}. The motor phase currents are sensed and are used to estimate the motor generated torque and the stator flux linkage [31]. The estimated torque T_{calc} and stator flux linkage λ_{calc} values are regulated to be the reference values T_{ref} and λ_{ref} using PI controllers ($K_p = 15$, 200 and $T_i = 0.1$, 0.002) to generate v_{qs} and v_{ds}, respectively. The obtained d-axis and q-axis voltages are transformed into the five-phase reference voltages using the transformation [32] and estimated rotor position "θ," which are further processed using the proposed DSACE PWM, as shown in Fig. 7.

V. Simulation Results and Experimental Verification

The simulation of the FPOEWIM drive system with the proposed decoupled and DSACE PWM techniques is performed using MATLAB/Simulink. The five-phase motor parameters used in the simulation are shown in Table III. The simulation is performed by considering the dc bus voltage of 100 V and 40 samples per fundamental cycle. Also, the deadtime between the top and the bottom switches of the inverter is considered to be 1 μs. The drive is operated with the open-loop V/f control under a no-load condition. Furthermore, the proposed PWM techniques

TABLE III
Nominal Parameters of FPOEWIM

Parameter	Value	Parameter	Value
Stator resistance (r_s)	1.05 Ω	Rotor resistance (r'_r)	1.42 Ω
Stator leakage inductance (L_{ls})	6 (mH)	Rotor leakage inductance (L'_{lr})	6 (mH)
Mutual inductance (M)	84.73 (mH)	Number of poles (P)	4
Moment of inertia (J)	0.148 (kg-m^2)	Nominal speed	1400 rpm

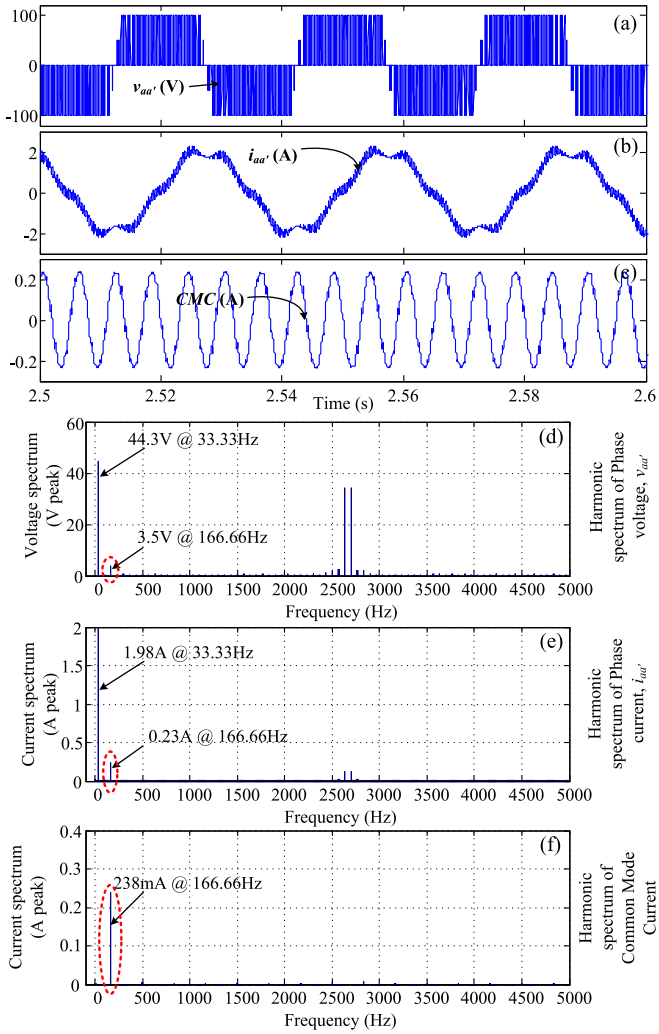

Fig. 9. Simulation results for the decoupled PWM technique. (a) FPOEWIM phase voltage. (b) Phase current. (c) Common mode current. Harmonic spectrum of (d) phase voltage, (e) phase current, and (f) CMC.

are operated in conjunction with the closed-loop DTC control technique and the results are presented using simulation studies.

Figs. 9 and 10 show the simulation results of the FPOEWIM drive system with the proposed decoupled and DSACE PWM techniques, respectively. These results are captured for the value of modulation index m_a set to 0.7. The motor phase voltage, phase current, and the CMC along with their harmonic spectrum are shown in Figs. 9 and 10. The encircled parts in the

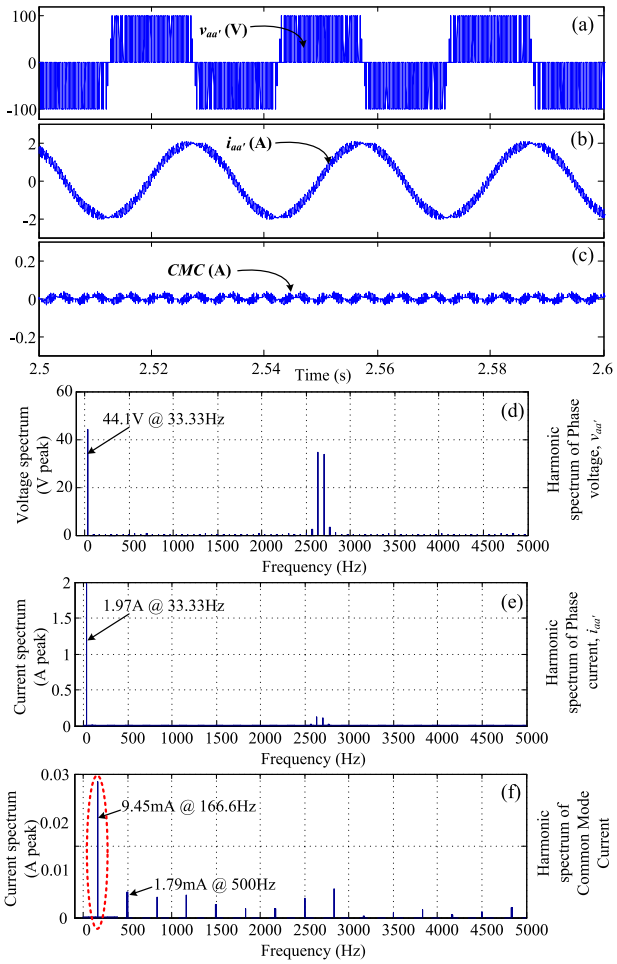

Fig. 10. Simulation results for the DSACE PWM technique. (a) FPOEWIM phase voltage. (b) Phase current. (c) CMC. Harmonic spectrum of (d) phase voltage, (e) phase current, and (f) CMC.

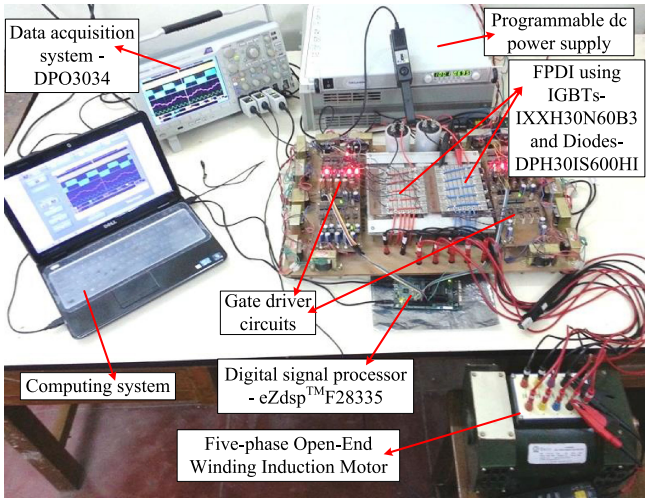

Fig. 11. Photograph of the experimental setup.

harmonic spectra of Fig. 9 show the fifth harmonic component of the respective voltage and currents. As the value of m_a is 0.7, the fundamental frequency is 33.33 Hz and the corresponding frequency of the fifth harmonic component is 166.66 Hz (see Fig. 9). So, the motor phase voltage and the phase current contain fifth harmonic component when the drive is operated with the decoupled PWM technique. The DSACE PWM technique eliminates the fifth harmonic component in the motor phase voltage and phase current, thereby eliminating the CMC and results in sinusoidal motor phase current, as shown in Fig. 10(b). It can be observed from the encircled part of the harmonic spectrum of the CMC in Fig. 10(f) that the value of CMC is nearly zero at 166.66 Hz. From Figs. 9 and 10, it can also be observed that both the PWM techniques eliminate the third harmonic content in the motor phase voltage and phase current.

To verify the simulation results, an experimental prototype is built, as shown in Fig. 11, and is operated using both the proposed decoupled and DSACE PWM techniques. Both the PWM techniques along with the open-loop V/ f control are tested under the no-load condition for the 1 HP, 100 V, 3.4 A, 50 Hz, 1400 r/min FPOEWIM whose parameters are given in Table III. The FPOEWIM is powered by a single programmable dc power supply *via* a custom made five-phase dual-inverter with a common dc bus. Ten independent gate pulses required to drive the top switches of the dual-inverter are generated using eZdspF28335 digital signal processor. The complementary gate pulses for the bottom devices are generated externally along with the deadtime of 1 μs between the top and bottom switches. The dc bus voltage of 100 V is applied and the waveforms are acquired using a Tektronix make 300-MHz DPO3034. The motor phase voltage is acquired using the differential probe, whereas the motor phase current is acquired using the current probe and the CMC is captured by passing both the positive and negative dc bus wires through a single current probe.

Fig. 12(a) shows the waveforms of the motor phase voltage, phase current, and the CMC (from top to bottom) when the FPOEWIM drive is operated with the decoupled PWM technique. All these waveforms are similar to the simulation results shown in Fig. 9. The corresponding harmonic spectra for all the above-discussed waveforms are shown in Fig. 12(b), (c), (d). The presence of a fifth harmonic component in the motor phase voltage and the phase current can be observed in Fig. 12(b) and (c). Also, the CMC is predominant at 166.66 Hz whose value is about 229 mA, which can be observed from the harmonic spectrum shown in Fig. 12(d).

Similarly, Fig. 13(a) shows the motor phase voltage, phase current, and the CMC when the drive is operated with the DSACE PWM technique. These waveforms are akin to the simulation results shown in Fig. 10. The sinusoidal nature of the motor phase current and nearly zero CMC depicts the effectiveness of the DSACE PWM technique. The suppression of fifth harmonic content in the motor phase voltage and the phase current can be observed from Fig. 13(b) and (c). Fig. 13(d) shows the harmonic spectrum for the CMC, where the magnitude of fifth harmonic component is about 12.5 mA, which is negligible when compared to the no-load current of the motor. In addition, the third harmonic content in the motor phase voltage and current is absent when both the proposed PWM techniques are employed.

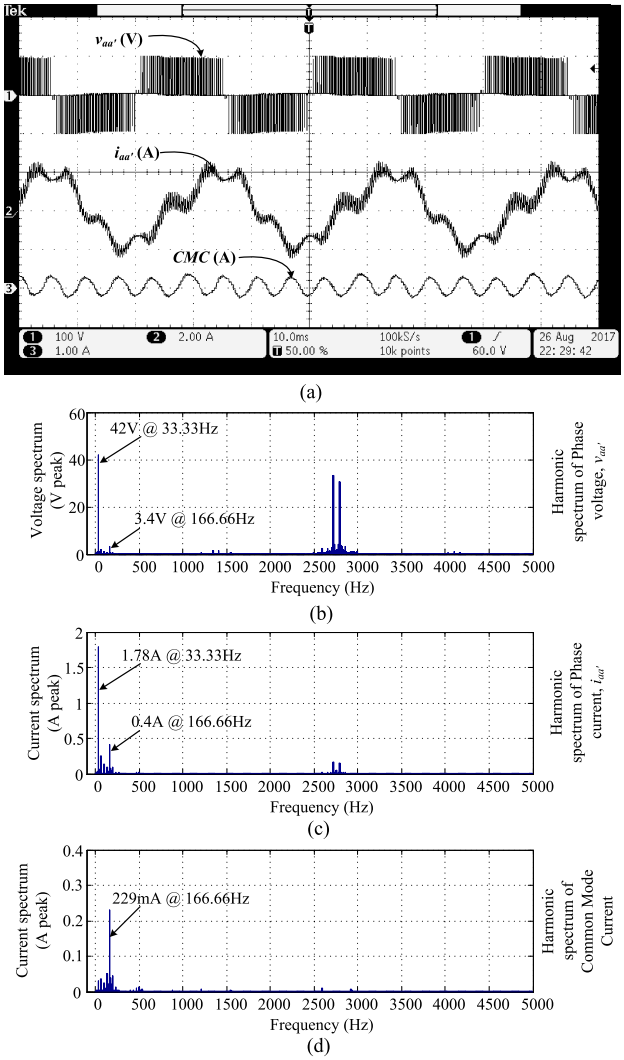

Fig. 12. Experimental results for the decoupled PWM technique: (top to bottom) phase-aa' voltage (y-axis: 100 V/div), phase-aa' current (y-axis: 2 A/div), and CMC (y-axis: 1 A/div) (x-axis: 10 ms/div). Harmonic spectrum of phase-aa' voltage, phase-aa' current, and CMC.

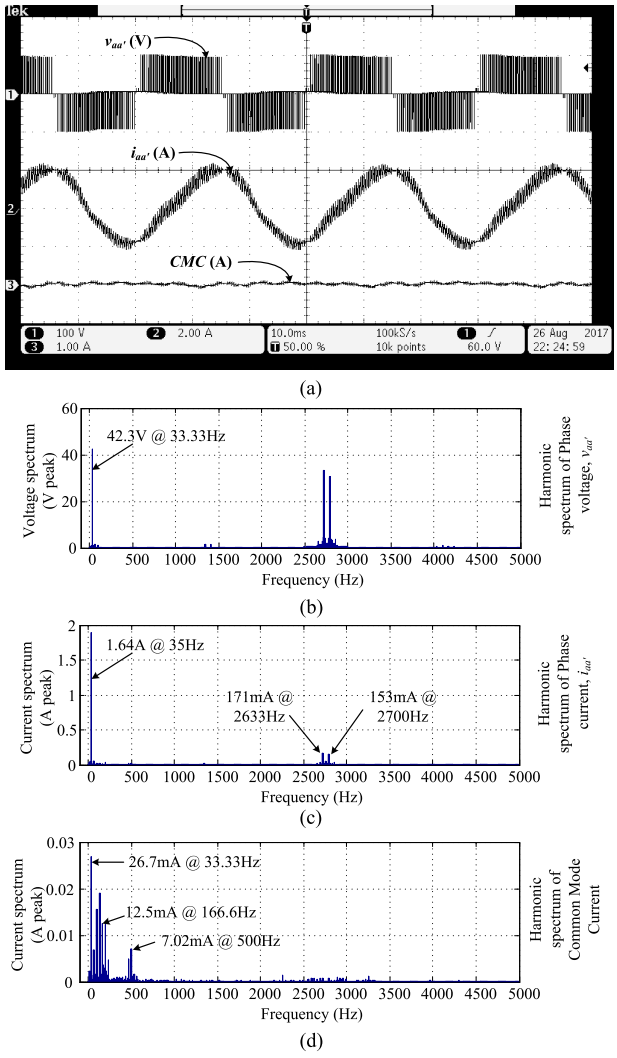

Fig. 13. Experimental results for the DSACE PWM technique: (top to bottom) phase-aa' voltage (y-axis: 100 V/div), phase-aa' current (y-axis: 2A/div), and CMC (y-axis: 1 A/div) (x-axis: 10 ms/div). Harmonic spectrum of phase-aa' voltage, phase-aa' current, and CMC.

The effectiveness of the proposed DSACE PWM technique is further verified by comparing the ripple content in the motor phase current and its THD with that of the 144° decoupled PWM technique. Another experiment for 144° decoupled PWM technique is carried out using the same experimental setup and similar conditions like dc bus voltage, deadtime, etc., are used.

The FPOEWIM is operated at a rated frequency of 50 Hz and no-load condition using both the 144° decoupled and DSACE PWM techniques and the phase-aa' voltage and current are captured, as shown in Figs. 14 and 15, respectively. From Fig. 14, it can be observed that the 144° decoupled PWM results in the harmonics near and around the switching frequency, whereas the DSACE PWM technique moves the harmonic content at twice the switching frequency. This could help in minimizing the filter size. From Fig. 15(a) and (b), it can be observed that the ripple content in the motor phase current is higher in case of 144° decoupled PWM when compared to that of the proposed DSACE PWM. The ripple content in the current Δi is shown in the zoomed-in parts. In addition, the harmonic spectrum of motor phase current for both the PWM techniques is shown in Fig. 15(c) and (d) for respective PWM techniques. From Fig. 15(c) and (d), it is evident that the reduction of ripple content in the current reduces its THD value. This is because of the reduction in the magnitude of high-frequency current components shown in the zoomed-in parts of the respective harmonic spectrum. Furthermore, the effect of ripple content in the current is shown in terms of THD, which is calculated for the frequency range of 5 to 50 Hz and is given in Fig. 16. From Fig. 16, it can be concluded that the proposed DSACE PWM technique results in lesser THD in the motor phase current when compared to the conventional 144° decoupled PWM technique. The current THD for 180° decoupled PWM is not shown in Fig. 16, since the current contains fifth-order harmonics that obviously results in higher THDs.

Furthermore, to verify the operation of the proposed DSACE PWM technique and to compare with 144° decoupled PWM

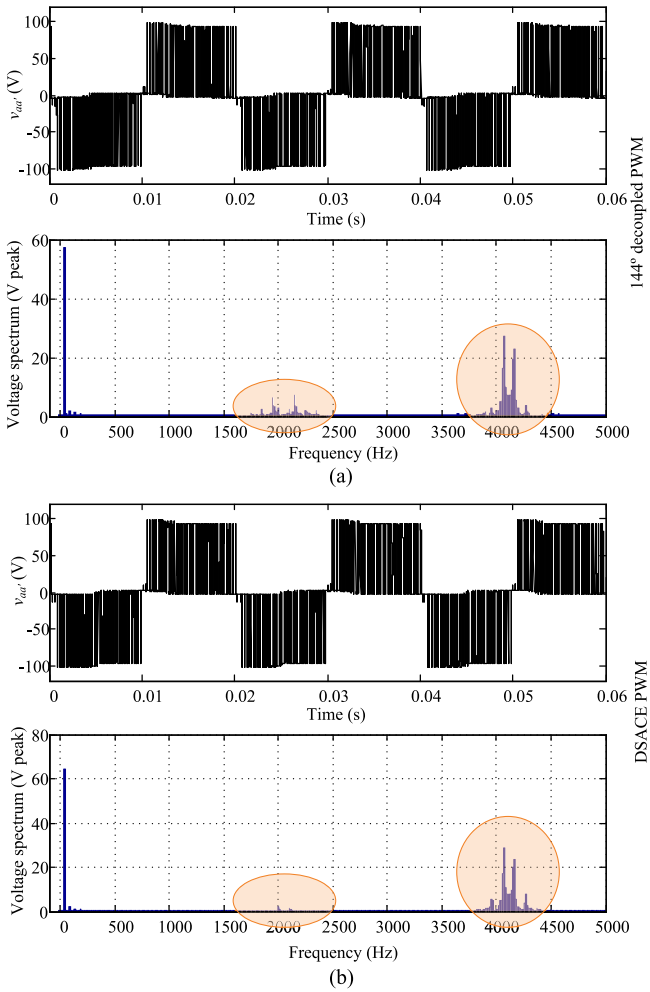

Fig. 14. Experiment results: FPOEWIM phase-aa' voltage. (a) Using 144° decoupled PWM technique. (b) Using DSACE PWM technique. Top plots are voltages and bottom plots are respective spectra.

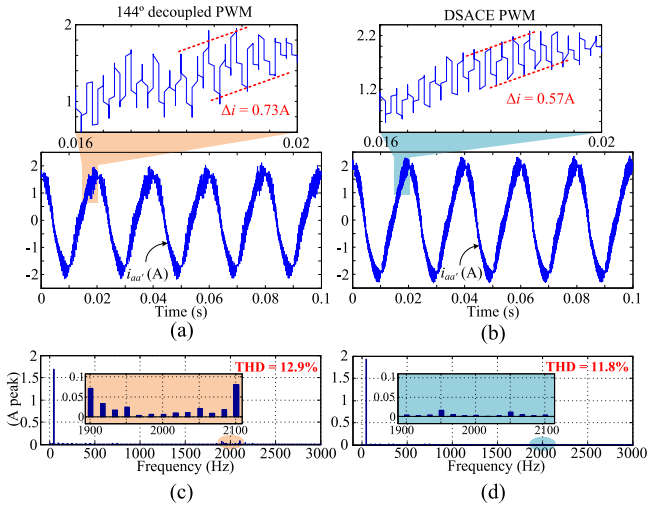

Fig. 15. Experiment results: FPOEWIM phase-aa' current. (a) Using 144° decoupled PWM technique. (b) Using DSACE PWM technique (top plots are zoomed-in plots from the bottom results). Harmonic spectrum of phase current. (c) Using 144° decoupled PWM technique. (d) Using DSACE PWM technique.

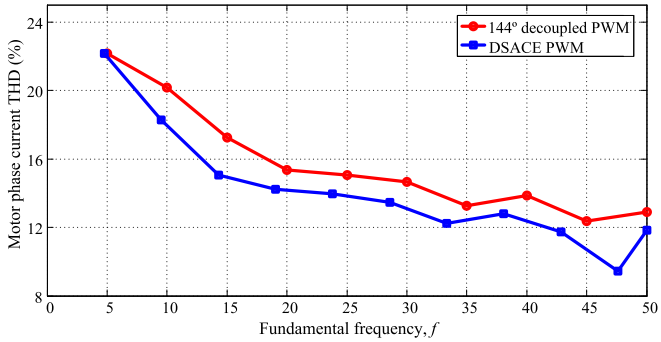

Fig. 16. Comparison of FPOEWIM phase current THDs for the proposed DSACE PWM techniques with the conventional 144° decoupled PWM technique.

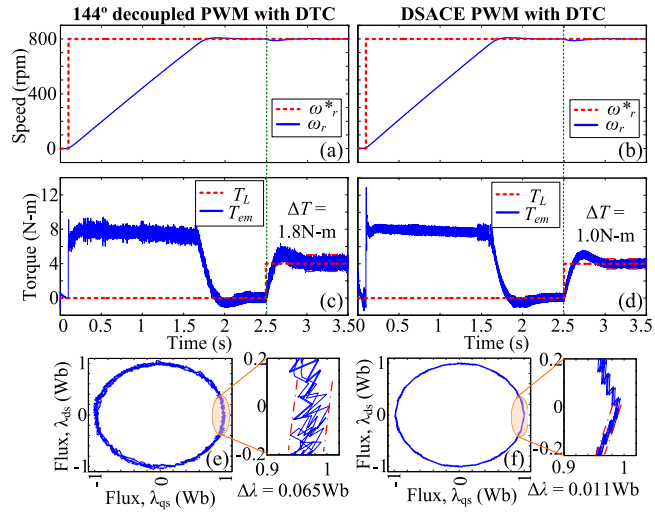

Fig. 17. Simulation results for the 144° decoupled PWM (left-hand side) and DSACE PWM (right-hand side) techniques in conjunction with DTC. (a) and (b) Motor speed. (c) and (d) Motor generated torque. (e) and (f) Flux trajectory.

technique in conjunction with the closed-loop DTC control technique, another simulation is performed using the schematic block diagram shown in Fig. 8. The motor speed (ω_r), generated torque (T_{em}), and the flux trajectories $(\lambda_{ds} - \lambda_{qs})$ of FPOEWIM operated with the 144° decoupled PWM technique and the proposed DSACE PWM along with the closed-loop DTC technique are shown in Fig. 17(a) and (f). The speed reference is set to 800 r/min at 0.1 s [see Fig. 17(a) and (b)]. The motor is initially operated under no-load condition, then the load of 4 N·m is applied at 2.5 s [see Fig. 17(c) and (d)]. The speed response is nearly same for both the PWM techniques, which can be observed from Fig. 17(a) and (b), so as the generated torque, as shown in Fig. 17(c) and (d). However, the ripple content in the generated torque is more if the 144° decoupled PWM technique (1.8 N·m) is used instead of the proposed DSACE PWM technique (1.0 N·m). This can also be supported with the higher ripple content in the flux trajectory shown in Fig. 17(e) when compared to that of Fig. 17(f) (also, see zoomed-in parts). Hence, the proposed DSACE PWM technique helps in reducing the ripple content in the motor generated torque.

VI. Conclusion

The decoupled and DSACE PWM techniques are proposed for the dual-inverter connected FPOEWIM drive with a single dc source. The detailed analysis and explanation of the proposed techniques is presented. The decoupled PWM technique results in a switching sequence, which varies from instant to instant in a sector. The switching sequence is chosen such that the reference voltage vector at every instant is realized by using the nearest possible SVLs. This reduces the ripple content in the motor phase current and hence the THD. But, the proposed 180° decoupled PWM technique results in CMC that is nullified using the DSACE PWM technique by retaining the property of the proposed PWM. The working of the proposed DSACE PWM technique is verified using the closed-loop DTC scheme and compared with the conventional 144° decoupled PWM technique. To conclude, the proposed DSACE PWM technique could eliminate the CMC and reduce the ripple content in the motor phase current. This could impact on the ripple content in the air-gap flux and the motor generated torque to avoid the torsional oscillations in the motor shaft.

References

[1] K. N. Pavithran, R. Parimelalagan, and M. R. Krishnamurthy, "Studies on inverter-fed five-phase induction motor drive," *IEEE Trans. Power Electron.*, vol. 3, no. 2, pp. 224–235, Apr. 1988.

[2] H. Xu, H. A. Toliyat, and L. J. Petersen, "Five-phase induction motor drives with DSP-based control system," *IEEE Trans. Power Electron.*, vol. 17, no. 4, pp. 524–533, Jul. 2002.

[3] R. Viju Nair, S. Arun Rahul, S. Pramanick, K. Gopakumar, and L. G. Franquelo, "Novel symmetric six-phase induction motor drive using stacked multilevel inverters with a single DC link and neutral point voltage balancing," *IEEE Trans. Ind. Electron.*, vol. 64, no. 4, pp. 2663–2670, Apr. 2017.

[4] K. Rahman, A. Iqbal, N. Al-Emadi, and L. Ben-Brahim, "Common mode voltage reduction in a three-to-five phase matrix converter fed induction motor drive," *IET Power Electron.*, vol. 10, no. 7, pp. 817–825, Jul. 2017.

[5] B. Tian, Q. T. An, J. D. Duan, D. Y. Sun, L. Sun, and D. Semenov, "Decoupled modeling and nonlinear speed control for five-phase PM motor under single-phase open fault," *IEEE Trans. Power Electron.*, vol. 32, no. 7, pp. 5473–5486, Jul. 2017.

[6] S. Payami, R. K. Behera, and A. Iqbal, "DTC of three-level NPC inverter fed five-phase induction motor drive with novel neutral point voltage balancing scheme," *IEEE Trans. Power Elect.*, vol. 33, no. 2, pp. 1487–1500, Feb. 2018.

[7] Y. N. Tatte and M. V. Aware, "Direct torque control of five-phase induction motor with common-mode voltage and current harmonics reduction," *IEEE Trans. Power Electron.*, vol. 32, no. 11, pp. 8644–8654, Nov. 2017.

[8] A. Nabae, I. Takahashi, and H. Akagi, "A new neutral-point-clamped PWM inverter," *IEEE Trans. Ind. Appl.*, vol. IA-17, no. 5, pp. 518–523, Sep./Oct. 1981.

[9] S. Payami, R. K. Behera, A. Iqbal, and R. Al-Ammari, "Common-mode voltage and vibration mitigation of a five-phase three-level NPC inverter-fed induction motor drive system," *IEEE J. Emerg. Sel. Topics Power Elect.*, vol. 3, no. 2, pp. 349–361, Jun. 2015.

[10] S. M. Ahmed, H. Abu-Rub, and Z. Salam, "Common-mode voltage elimination in a three-to-five-phase dual matrix converter feeding a five-phase open-end drive using space-vector modulation technique," *IEEE Trans. Ind. Electron.*, vol. 62, no. 10, pp. 6051–6063, Oct. 2015.

[11] N. Bodo, M. Jones, and E. Levi, "A space vector PWM with common-mode voltage elimination for open-end winding five-phase drives with a single DC supply," *IEEE Trans. Ind. Electron.*, vol. 61, no. 5, pp. 2197–2207, May 2014.

[12] N. Ky Nguyen, F. Meinguet, E. Semail, and X. Kestelyn, "Fault-tolerant operation of an open-end winding five-phase PMSM drive with short-circuit inverter fault," *IEEE Trans. Ind. Electron.*, vol. 63, no. 1, pp. 595–605, Jan. 2016.

[13] P. P. Rajeevan, H. Abu-Rub, A. Iqbal, and K. Gopakumar, "Common mode voltage elimination scheme for dual-inverter fed five phase AC drives with open-end stator windings," in *Proc. IEEE Int. Conf. Ind. Technol.*, 2013, pp. 1680–1685.

[14] H. Stemmler and P. Guggenbach, "Configurations of high-power voltage source inverter drives," in *Proc. 5th Eur. Conf. Power Electron. Appl.*, 1993, pp. 7–12.

[15] A. Edpuganti and A. K. Rathore, "New optimal pulsewidth modulation for single DC-link dual-inverter fed open-end stator winding induction motor drive," *IEEE Trans. Power Electron.*, vol. 30, no. 8, pp. 4386–4393, Aug. 2015.

[16] B. V. Reddy and V. T. Somasekhar, "An SVPWM scheme for the suppression of zero-sequence current in a four-level open-end winding induction motor drive with nested rectifier–inverter," *IEEE Tran. Ind. Electron.*, vol. 63, no. 5, pp. 2803–2812, May 2016.

[17] V. T. Somasekhar, K. Gopakumar, and E. G. Shivakumar, "A space-vector modulation scheme for a dual two-level inverter fed open-end winding induction motor drive for the elimination of zero-sequence currents," *EPE J.*, vol. 12, no. 2, pp. 1–19, 2002.

[18] V. Oleschuk, A. Sizov, B. K. Bose, and A. M. Stankovic, "Phase-shift-based synchronous modulation of dual inverters for an open-end winding motor drive with elimination of zero sequence currents," in *Proc. Int. Conf. Power Elect. Drives Syst.*, 2005, pp. 325–330.

[19] V. T. Somasekhar, S. Srinivas, B. P. Reddy, C. N. Reddy, and K. Sivakumar, "Pulse-width-modulated switching strategy for the dynamic balancing of zero-sequence current for a dual-inverter fed open-end winding induction motor drive," *IET Elect. Power Appl.*, vol. 1, no. 4, pp. 591–600, Jul. 2007.

[20] S. Jain, R. Karampuri, and V. T. Somasekhar, "An integrated control algorithm for a single-stage PV pumping system using an open-end winding induction motor," *IEEE Trans. Ind. Electron.*, vol. 63, no. 2, pp. 956–965, Feb. 2016.

[21] D. Wu, X. Wu, L. Su, X. Yuan, and J. Xu, "A dual three-level inverter-based open-end winding induction motor drive with averaged zero-sequence voltage elimination and neutral-point voltage balance," *IEEE Trans. Ind. Electron.*, vol. 63, no. 8, pp. 4783–4795, Aug. 2016.

[22] V. T. Somasekhar, S. Srinivas, and K. K. Kumar, "Effect of zero-vector placement in a dual inverter fed open-end winding induction motor drive with a decoupled space-vector PWM strategy," *IEEE Trans. Ind. Elect.*, vol. 55, no. 6, pp. 2497–2505, Jun. 2008.

[23] S Jain, A. Kumar, R. Karampuri, and V. T. Somasekhar, "A single-stage photovoltaic system for a dual-inverter fed open-end winding induction motor drive for pumping applications," *IEEE Trans. Power Elect.*, vol. 30, no. 9, pp. 4809–4818, Sep. 2015.

[24] R. Karampuri, S. Jain, and V. T. Somasekhar, "Phase displaced SVPWM technique for five-phase open-end winding induction motor drive," in *Proc. IEEE Students' Conf. Elect. Electron. Comput. Sci.*, Bhopal, India, 2016, pp. 1–6.

[25] R Karampuri, S. Jain, and V. T. Somasekhar, "Sample-averaged zero-sequence current elimination PWM technique for five-phase induction motor with opened stator windings," *IEEE J. Emerg. Sel. Topics Power Elect.*, vol. 6, no. 2, pp. 864–873, Jun. 2018.

[26] R. Karampuri, J. Prieto, F. Barrero, and S. Jain, "Extension of the DTC technique to multi-phase induction motor drives using any odd number of phases," in *Proc. IEEE Veh. Power Propulsion Conf.*, Coimbra, Portugal, Oct. 2014, pp. 1–6.

[27] D.-W. Chung, J.-S. Kim, and S.-K. Sul, "Unified voltage modulation technique for real-time three-phase power conversion," *IEEE Trans. Ind. Appl.*, vol. 34, no. 2, pp. 374–380, Mar./Apr. 1998.

[28] H. Gao, J. Su, G. Yang, and J. Liu, "SVPWM equivalent algorithm based on carrier for five-phase voltage source inverter," in *Proc. Conf. 7th Int. Power Electron. Motion Control Conf.*, 2012, pp. 758–762.

[29] H.-M. Ryu, J.-H. Kim, and S.-K. Sul, "Analysis of multiphase space vector pulse-width modulation based on multiple d–q spaces concept," *IEEE Trans. Power Elect.*, vol. 20, no. 6, pp. 1364–1371, Nov. 2005.

[30] B. R. Vinod, M. R. Baiju, and G. Shiny, "Five-level inverter fed space vector based direct torque control of open-end winding induction motor drive," *IEEE Trans. Energy Convers.*, vol. 33, no. 3, pp. 1392–1401, Sep. 2018.

[31] H. Miranda, P. Cortés, J. I. Yuz, and J. Rodríguez, "Predictive torque control of induction machines based on state-space models," *IEEE Trans. Ind. Electron.*, vol. 56, no. 6, pp. 1916–1924, Jun. 2009.

[32] R. Karampuri, J. Prieto, F. Barrero, and S. Jain, "A comparison between FOC and DTC methods for five-phase induction motor drives," in *Proc. Conf. 11th Int. Conf. Model. Simul. Elect. Mach., Converters Syst.*, Valencia, Spain, May 2014.

Authors' photographs and biographies not available at the time of publication.